BBA - Biomembranes 1863 (2021) 183725

Contents lists available at ScienceDirect

BBA - Biomembranes

journal homepage: www.elsevier.com/locate/bbamem

Solubilization of artificial mitochondrial membranes by amphiphilic copolymers of different charge

Kevin Janson [a,b], Jennifer Zierath [b], Fotis L. Kyrilis [a,b], Dmitry A. Semchonok [a], Farzad Hamdi [a], Ioannis Skalidis [a,b], Adrian H. Kopf [c], Manabendra Das [d], Cenek Kolar [e], Marie Rasche [e], Carolyn Vargas [d,f,g,h], Sandro Keller [d,f,g,h], Panagiotis L. Kastritis [a,b,i,*], Annette Meister [a,b,*]

[a] Interdisciplinary Research Center HALOmem, Charles Tanford Protein Center, Martin Luther University Halle-Wittenberg, Kurt-Mothes-Straße 3a, 06120 Halle/Saale, Germany
[b] Institute of Biochemistry and Biotechnology, Martin Luther University Halle-Wittenberg, Kurt-Mothes-Straße 3a, 06120 Halle/Saale, Germany
[c] Membrane Biochemistry and Biophysics, Bijvoet Center for Biomolecular Research, Institute of Biomembranes, Utrecht University, Padualaan 8, 3584 CH Utrecht, the Netherlands
[d] Molecular Biophysics, Technische Universität Kaiserslautern (TUK), Erwin-Schrödinger-Straße 13, 67663 Kaiserslautern, Germany
[e] GLYCON Biochemicals GmbH, Im Biotechnologie Park TGZ 1, 14943 Luckenwalde, Germany
[f] Biophysics, Institute of Molecular Biosciences (IMB), NAWI Graz, University of Graz, Humboldtstr. 50/III, 8010 Graz, Austria
[g] Field of Excellence BioHealth, University of Graz, Graz, Austria
[h] BioTechMed-Graz, Graz, Austria
[i] Biozentrum, Martin Luther University Halle-Wittenberg, Weinbergweg 22, 06120 Halle/Saale, Germany

ARTICLE INFO

Keywords:
Polymer nanodiscs
DIBMA
SMA
Inner mitochondrial vesicles
Transmission electron microscopy

ABSTRACT

Certain amphiphilic copolymers form lipid-bilayer nanodiscs from artificial and natural membranes, thereby rendering incorporated membrane proteins optimal for structural analysis. Recent studies have shown that the amphiphilicity of a copolymer strongly determines its solubilization efficiency. This is especially true for highly negatively charged membranes, which experience pronounced Coulombic repulsion with polyanionic polymers. Here, we present a systematic study on the solubilization of artificial multicomponent lipid vesicles that mimic inner mitochondrial membranes, which harbor essential membrane-protein complexes. In particular, we compared the lipid-solubilization efficiencies of established anionic with less densely charged or zwitterionic and even cationic copolymers in low- and high-salt concentrations. The nanodiscs formed under these conditions were characterized by dynamic light scattering and negative-stain electron microscopy, pointing to a bimodal distribution of nanodisc diameters with a considerable fraction of nanodiscs engaging in side-by-side interactions through their polymer rims. Overall, our results show that some recent, zwitterionic copolymers are best suited to solubilize negatively charged membranes at high ionic strengths even at low polymer/lipid ratios.

1. Introduction

After the first application of an amphiphilic copolymer for membrane-protein isolation in 2009 by Knowles et al. [1], numerous synthetic efforts have been undertaken to substitute classical detergents by copolymers for membrane solubilization [2–6]. The main drawback of detergent-based extraction is the destabilization of the protein of interest, since detergent molecules completely or at least partly replace the protein-surrounding lipids [7]. By contrast, amphiphilic copolymers such as styrene/maleic acid (SMA) and diisobutylene/maleic acid (DIBMA) wrap around discoidal membrane patches maintaining the membrane proteins in their local lipid environment [8]. The nanodiscs (NDs) thus formed are suitable for structural studies, especially for structure determination of integral membrane proteins using single-particle cryo-electron microscopy (cryo-EM) [6,9–13]. The advantage of retaining the membrane architecture, including the local lipid composition, resulted in the development of two main copolymer classes, SMA and DIBMA (Fig. 1) [8,14,15], including various functionalized variants. Tremendous efforts have been undertaken to expand their scope of application towards broader pH intervals and high ionic

* Corresponding authors at: Interdisciplinary Research Center HALOmem, Charles Tanford Protein Center, Martin Luther University Halle-Wittenberg, Kurt-Mothes-Straße 3a, 06120 Halle/Saale, Germany.
E-mail addresses: panagiotis.kastritis@bct.uni-halle.de (P.L. Kastritis), annette.meister@chemie.uni-halle.de (A. Meister).

https://doi.org/10.1016/j.bbamem.2021.183725
Received 1 May 2021; Received in revised form 21 July 2021; Accepted 2 August 2021
Available online 10 August 2021

strength as well as to minimize deleterious Coulombic repulsion between the polymer and membrane lipids [16–20]. An increasing number of quantitative studies discuss how lipid composition and phase state as well as lipid net charge determine solubilization efficiency [21–25]. Recently, new synthetic copolymers with hydrophobic [26,27] and zwitterionic side chains [28] have shown improved solubilization properties. However, the complexity of the solubilization process hinders a detailed understanding of all factors influencing membrane solubilization and nanodisc formation. On the one hand, biological membranes are much more complex systems than artificial membranes (e.g., vesicles). Their lipid and protein composition as well as net charge depend on the organism at hand and on the cellular state that dictates buffer conditions, pH, and ionic strength to work with. On the other hand, the impact of amphiphilic copolymers on membranes depends on the polymers' hydrophobic/hydrophilic balance, net charge, sequence, length, and composition of the side chains. Thus, solubilization efficiency, as well as nanodisc size and shape, are difficult to predict or even control, since they strongly depend on the above-mentioned factors.

The choice of the appropriate lipid membrane for ND formation is driven by the question to be answered. Natural membranes, being composed of complex mixtures of lipids and membrane proteins, are usually applied for structural investigations (e.g., electron microscopy [6,29]), and information about their lipid composition has been studied using thin-layer chromatography or mass spectrometry [30–33]. By contrast, artificial model membranes are devoid of membrane proteins. They are composed of one or just a few synthetic lipids that frequently serve for physicochemical studies on the formed NDs [5,24,26,34]. A few authors apply more native-like lipid extracts to discuss lipid-dependent ND formation [6,35–37].

The aim of this study was to investigate the solubilization of artificial model membranes mimicking the natural membrane lipid composition of inner mitochondrial membranes. These multicomponent membranes contain a high amount of cardiolipin (CL) and are known to withstand solubilization by the commonly used polymer SMA up to mass ratios of polymer (P) to lipid (L) of $m_P/m_L = 3$ [2]. To increase the solubilization efficiency, we applied recently developed copolymers of negative, positive, or zero net charge (see Fig. 1). Highly specialized mitochondrial membranes form tube-like extensions of large sheet-like cristae [40]. Strain imposed by the high curvature is relieved by an asymmetric distribution of phospholipids in the lumen- and matrix-facing leaflets with cardiolipin (~18 mol%) and phosphatidylethanolamine (~34 mol%) segregated to the negatively curved monolayer leaflet facing the crista lumen [41–44]. By replacing or omitting CL in artificial vesicle preparations mimicking the inner mitochondrial membrane composition of mammalian heart, we studied the role of CL in the solubilization process using dynamic light scattering (DLS) and transmission electron microscopy (TEM). Our results show that zwitterionic copolymers are best suited to solubilize negatively charged membranes at high ionic strength even at low polymer/lipid ratios.

2. Materials and methods

2.1. Materials

The lipid components of the artificial inner mitochondrial lipid mixtures (IMLMs) mimicking the membranes of pig (*Sus scrofa*) heart and yeast (*Saccharomyces cerevisiae*) were purchased from Avanti Polar Lipids (Alabaster, USA). For pig heart membranes, they comprise bovine heart L-α-phosphatidylcholine (PC), bovine heart L-α-phosphatidylethanolamine (PE), bovine liver L-α-phosphatidylinositol sodium salt (PI), bovine heart cardiolipin, sodium salt (CL), and soy L-α-phosphatidylglycerol sodium salt (PG). Each of the natural lipids contains a mixture of di-saturated, di-unsaturated, and saturated/unsaturated fatty acyl chains (see Fig. S1). For mimicking *S. cerevisiae* membranes, we used 1-palmitoyl-2-oleoyl-*sn*-glycero-3-phosphocholine (POPC), 1-palmitoyl-2-oleoyl-*sn*-glycero-3-phosphoethanolamine (POPE), 1-palmitoyl-2-oleoyl-*sn*-glycero-3-phosphoinositol (ammonium salt) (POPI), 1-palmitoyl-2-oleoyl-*sn*-glycero-3-phospho-L-serine (sodium salt) (POPS), and 1′,3′-bis[1-palmitoyl-2-oleoyl-*sn*-glycero-3-phospho]-glycerol (sodium salt) (16:0–18:1 CL).

SMA(2:1) hydrolysed from styrene/maleic anhydride (2:1) (tradename Xiran SZ30010) was kindly provided by Polyscope (Geleen, Netherlands). DIBMA (tradename Sokalan CP 9) was a kind gift from BASF (Ludwigshafen, Germany). SB-DIBMA (sulfobetaine DIBMA) was synthesized from diisobutylene-maleic anhydride (2:1) reacting with *N*, *N*-dimethyl-1,3-propanediamine to form a maleimide, which was further reacted with propane sultone to afford the final product. Glyco-DIBMA was synthesized as described before; briefly, DIBMA anhydride was amidated with *N*-methyl-D-glucamine (meglumine) in a refluxing methanolic solution of sodium. Styrene-maleimide quaternary ammonium (QA1-SMA(2:1) and QA2-SMA(2:1)) was synthesized as described in [39], starting from styrene-maleic anhydride (SMAnh 2:1, tradename Xiran SZ30010). In the two-step process, the anhydride was first reacted with (2-aminoethyl)- or (2-aminopropyl)-trimethylammonium chloride hydrochloride and subsequently the resulting maleimide was formed. Tris and NaCl were purchased from Sigma-Aldrich (Karlsruhe, Germany). Water was ultrapure Millipore quality (conductivity <0.055 μS/cm, total organic carbon (TOC) < 5 ppm).

2.2. Preparation of vesicles

Lipid mixtures were prepared directly from the lipid stock solutions in chloroform by combining appropriate volumes. The organic solvent was removed in a stream of nitrogen. Residual traces of solvent were

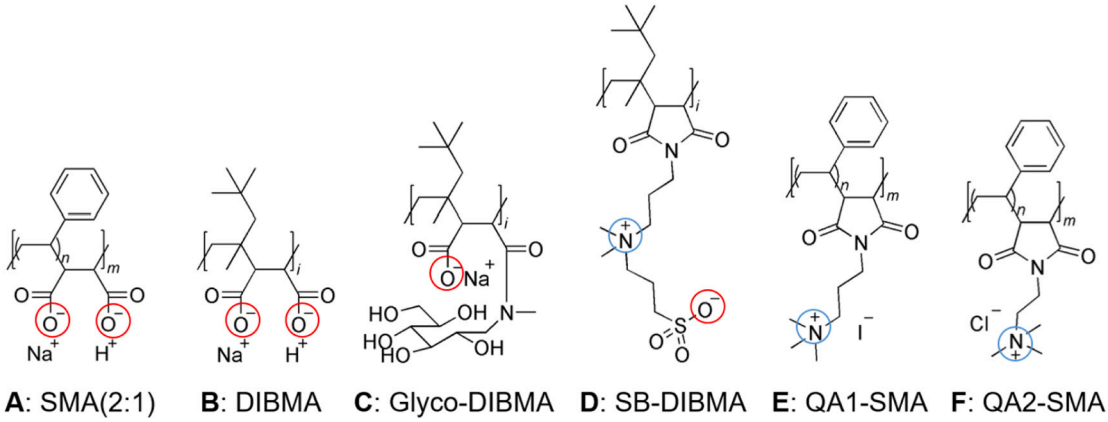

Fig. 1. Chemical structure of amphiphilic copolymers. (A–C) Anionic SMA(2:1) [8,21], DIBMA [22], Glyco-DIBMA [38]; (D) zwitterionic SB-DIBMA; (E–F) cationic QA1-SMA(2:1), QA2-SMA(2:1) [39] with n $i \approx 37$, $n \approx 2$, and $m \approx 7$.

eliminated under vacuum within 8 h. Aliquots, with lipid mixtures of 1 mg of lipid were stored at −80 °C under argon atmosphere. Lipid aliquots were suspended in 50 mM Tris buffer (pH 7.4) containing 200 or 500 mM of NaCl, respectively, just before use. The final lipid concentration was 1 mg/mL. Suspensions were vortexed for 5 min at 22 °C followed by 11-fold extrusion through a polycarbonate membrane with a nominal pore diameter of 100 nm using a Mini-Extruder (Avanti, Alabama, USA). The formation of large unilamellar vesicles (LUVs) was verified by DLS, yielding hydrodynamic LUV diameters of ~160 nm.

2.3. Preparation of copolymer stock solutions

The commercial copolymer solutions SMA(2:1) and DIBMA (~3 mL) were dialyzed against 1 L buffer using a 5-mL QuixSep dialyzer (Carl Roth, Karlsruhe, Germany) and a ZelluTrans dialysis membrane (Carl Roth, Karlsruhe, Germany) with a nominal molar-mass cutoff of 3.5 kg/mol. Dialysis was carried out at room temperature for 24 h with buffer exchange after 12–16 h. Recovered copolymers were filtered through 220-nm cellulose mix filters (Carl Roth, Karlsruhe, Germany) and stored at 22 °C. Copolymer stock concentrations were determined by refractometry on an Abbemat 3200 instrument (Anton Paar, Graz, Austria). The molar and mass concentrations of SMA(2:1) and DIBMA were calculated using the molar and mass refractive index increments, dn/dc, described in the literature [14,21].

Stock solutions of SB-DIBMA, Glyco-DIBMA, QA1-SMA(2:1), and QA2-SMA(2:1) were prepared by weighing in an appropriate amount of polymer on a high-precision XPR56 microbalance (Mettler Toledo, Gießen, Germany) into a glass vial followed by addition of an appropriate amount of buffer (pH 7.4, 50 mM Tris and 200 or 500 mM NaCl, respectively). The suspensions were sonicated at 70 °C using an ultrasonic bath (Elma Schmidbauer, Singen, Germany) until the samples appeared clear. Polymer stock solutions were then passed through 220-nm cellulose mix filters (Carl Roth, Karlsruhe, Germany) and stored at 22 °C. Copolymer concentrations were determined by refractometry on an Abbemat 3200 instrument (Anton Paar, Graz, Austria). The mass concentrations were calculated using the mass refractive index increment, dn/dρ, of SB-DIBMA and Glyco-DIBMA [38] and based on the initial weight of QA1-SMA(2:1) and QA2-SMA(2:1).

2.4. Preparation of nanodiscs

Nanodiscs were prepared by adding the copolymer solution (5% (w/v)) to vesicles that were prepared in the same buffer (pH 7.4) containing 50 mM Tris and 200 or 500 mM NaCl, respectively. Mass ratios of polymer (P) to lipid (L) of $m_P/m_L = 0.25–10$, and lipid concentrations between 0.25 and 0.5 mg/mL were used. These mixtures were incubated for 16 h at 35 °C. All preparations were performed in triplicate.

2.5. Dynamic light scattering

DLS measurements were carried out on a Litesizer 500 instrument (Anton Paar, Graz, Austria) equipped with a 633-nm He-Ne laser and a detection angle of 90°. Samples were thermostatted for 2 min at 25 °C before measurements were performed in a 1.5-mL disposable PMMA cuvette with a cross-section of 12.5 mm × 12.5 mm (Brand, Wertheim, Germany). Each sample was measured 6 times. Effects of buffer components and concentrations on the viscosity and RI of the solvent were accounted for during data analysis. Autocorrelation functions were fitted applying the Kalliope software (Anton Paar, Graz, Austria) using a non-negatively constrained least-squares function [45], which is further regularized by a so-called Tikhonov regularization [46] to yield intensity-weighted particle size distributions and by cumulant analysis [47] to obtain z-average particle diameters and associated polydispersity indices (PDIs). Distribution widths of z-average diameters, σ, were calculated as $\sigma = \sqrt{\mathrm{PDI}}\, z$ [48]. In the case of multimodal distributions, the hydrodynamic particle diameter was taken as the position of the first peak corresponding to the smallest size, which is justified by the steep dependence of light scattering intensity on particle size.

2.6. Negative-stain transmission electron microscopy

EM grids were prepared by loading 10 μL polymer-bounded nanodiscs (0.05 mg/mL lipid) onto glow-discharged copper TEM grids with continuous 10–12 nm carbon film coating (300 mesh size; Quantifoil Micro Tools, Großlöbichau, Germany). Excess liquid was blotted off with a strip of filter paper after 45 s followed by two washing steps and staining with 5 μL 2% (w/v) aqueous uranyl acetate solution. Specimens were dried and examined in an EM 900 transmission electron microscope (Carl Zeiss Microscopy, Oberkochen, Germany), and micrographs were recorded with an SM-1k-120 slow-scan charge-coupled device (slow-scan CCD) camera (TRS, Moorenweis, Germany). Selected specimens were imaged using a 200 keV Glacios Cryo-Transmission Electron Microscope equipped with a Falcon IIIEC direct electron detector (ThermoFisher Scientific, Oregon, USA).

2.7. Image processing of negative-stain data and size calculations

About 660 images, acquired with a total dose of 30 $e^-/Å^2$ and pixel size of 0.9612 Å, of negatively stained samples were processed in Relion 3.0 [49]. Micrographs were collected in 15 fraction movies and the fractions were motion corrected, averaged and dose weighted using MotionCor2 software [50]. Contrast Transfer Function (CTF) parameters including estimation of the defocus and astigmatism were evaluated by Gctf [51]. The CTF fitting of each micrograph was examined and screened by checking the Thon ring fitting accuracy manually. The micrographs with a low CTF resolution were discarded [51]. Manually picked 37,623 particles proceeded for the 2D classification with 100 classes. From these resulted 100 2D class averages, 39 of 2D class averages containing 83.46% (31,401 particles) of all picked particles were selected for further analysis. Particles size measurements were done in FIJI [52]. The minimum and the maximum diameter of the particles were measured and subsequently used to calculate the average diameter of the particles.

2.8. Cryo transmission electron microscopy

Cryo-EM grids were prepared by applying samples to glow-discharged Lacey (300 mesh, PLANO, Wetzlar, Germany) and holey carbon grids (Quantifoil R1.2/1.3, 200 mesh). Vitrification was performed using the Vitrobot Mark IV system (Thermo Fisher Scientific) with 95% humidity and a blotting time of 4 s. Specimen were examined at 200 keV with a Thermo Scientific Glacios Cryo-Transmission Electron Microscope equipped with a Falcon IIIEC direct electron detector in low dose mode.

3. Results & discussion

3.1. Morphology of lipid vesicles mimicking inner mitochondrial membranes (pig heart)

The vesicles used for solubilization experiments were prepared from inner mitochondrial lipid mixtures, which mimic pig heart inner mitochondrial membranes in terms of lipid head group composition and fatty acid chain length [44,53] (Fig. S1, Tables 1, 2). To examine the role of CL during solubilization, vesicles with CL (IMLM+CL), without CL (IMLM), with phosphatidylglycerol (PG) instead of CL (IMLM+PG), and without the negatively charged lipids CL and PI (IMLMneutral) were investigated (Fig. S1, Table 1).

The main component of IMLM+CL is with 40 mol% the zwitterionic phosphatidylethanolamine (PE), followed by 28 mol% zwitterionic

Table 1
Lipid headgroup distribution of pig heart inner mitochondrial membranes [44] and IMLM artificial inner mitochondrial lipid mixtures.[a]

Lipid headgroup	Pig heart inner mitochondrial membrane[b]		IMLM+CL	IMLM	IMLM+PG	IMLM neutral
PC	26.5	Heart-PC	28	38.35	17.65	41.2
PE	38.0	Heart-PE	40	54.8	25.2	58.8
PI	3.4	Liver-PI	5	6.85	3.15	–
CL/PA	25.4	Heart-CL	27	–	Soy-PG: 54	–

[a] All values are given in mol%.
[b] Includes 2% Lyso-PC/PE and 4.7% unknown components.

Table 2
Solubilization of artificial inner mitochondrial membrane vesicles with DIBMA at different polymer to lipid mass ratios. Crosses indicate ND formation based on DLS and negative-stain EM.

Lipid mix	IMLM+CL		IMLM+PG		IMLM		IMLMneutral	
m_P/m_L (g/g)	c_{NaCl} (mM)							
	200	500	200	500	200	500	200	500
1.5						×		×
3.5						×		×
5						×		×
7						×		×
10	×	×		×	×	×	×	×

P = DIBMA; L = lipid mixture.

phosphatidylcholine (PC), 27 mol% CL with two negative charges [54], and the minor component phosphatidylinositol (PI) with one negative charge (5 mol%) (Table 1). The acyl chain lengths of these lipids vary between C16 and C20 with different levels of unsaturation (C18:1, C18:2, and C20:4) (Table S1, Fig. S2).

The shape of the formed vesicles strongly depends on the geometry or "packing properties" of the lipids described by the packing parameter $P = v / a_0 l_c$ with the head group area a_0, the volume v of the hydrocarbon chain or chains, and their critical length l_c [55]. PC, PI, and PG lipids with unsaturated acyl chains and large headgroups have packing parameters of $P \approx 1$ corresponding to a cylindrical shape that favors the formation of flat bilayer sheets or large vesicles with low curvature.

According to Israelachvili [55], PE and CL lipids with unsaturated acyl chains have P values larger than 1, pointing to an inverted truncated cone shape of the lipids (Fig. S1) and preferring the inner leaflet of 100 nm-vesicles [56]. On the one hand, high amounts of PE favor the formation of multilamellar vesicles since the zwitterionic PE headgroup acts as donor and acceptor for inter- and intramolecular hydrogen bonds [57]. On the other hand, electrostatic repulsion between charged bilayers prevents the formation of multilamellar vesicles. Since IMLM+CL contains both high amounts of PE as well as negatively charged CL and PI, we expect the coexistence of uni- and multilamellar vesicles. The cryo-EM images in Fig. 2A–D show that most of the extruded vesicles had diameters between 80 and 200 nm. In addition, no clear preference for unilamellar or multilamellar vesicles was observed, as expected. The lipids of all mixtures were in the liquid-crystalline state forming smooth, spherical vesicles without any facets.

The size of the formed vesicles was confirmed by dynamic light scattering. The artificial inner mitochondrial lipid mixtures form vesicles with hydrodynamic diameters of (162 ± 3) nm (IMLM+CL), (170 ± 10) nm (IMLM+PG), (158 ± 10) nm (IMLM), and (156 ± 5) nm (IMLMneutral), respectively (Fig. S3). The formation of vesicles with diameters larger than 100 nm might be explained by the lipid composition, favoring low curvatures, since 33% (IMLM+CL) and up to 75% (IMLM+PG) of the lipids have P values equal to 1 (Fig. S1). As a consequence, vesicles deform during extrusion through polycarbonate membranes with a nominal pore diameter of 100 nm, but, after passage, maintain their larger diameters.

3.2. Solubilization of lipid vesicles mimicking inner mitochondrial membranes (pig heart) with DIBMA

The ability of DIBMA to solubilize inner mitochondrial membranes was studied by subjecting artificial inner mitochondrial membrane vesicles of different compositions to increasing polymer concentrations in the presence of NaCl (Table 3). The formation of NDs was monitored by DLS and negative-stain EM (Figs. 3, 4). Table 2 summarizes the solubilization trials for IMLM+CL, IMLM+PG, IMLM, and IMLMneutral at mass ratios of polymer (P) to lipid (L) of m_P/m_L = 1.5, 3.5, 5, 7, and 10, and at NaCl concentrations of 200 and 500 mM, respectively.

DLS results are summarized for the lowest and highest m_P/m_L ratios at which NDs could be detected (Fig. 3). Intensity-weighted particle size distributions show the coexistence of NDs and original vesicles for all investigated lipid mixtures marked with "X" in Table 2. From the multimodal distributions, the hydrodynamic particle diameter was taken as the position of the first peak corresponding to the smallest size, which is justified by the strong dependence of light scattering intensity on particle size. The z-average hydrodynamic diameter and the associated size distribution width of the formed NDs varies between d_z = (8 ± 3) nm (IMLM-PG) and d_z = (11 ± 6) nm (IMLM-neutral) (Fig. 3). The observed ND sizes are somewhat smaller than those reported for DIBMA-solubilized DMPC, which we ascribe to differences in lipid composition, especially the use of charged natural lipids with unsaturated acyl chains [14].

A detailed discussion of the observed ND diameter is hindered by the

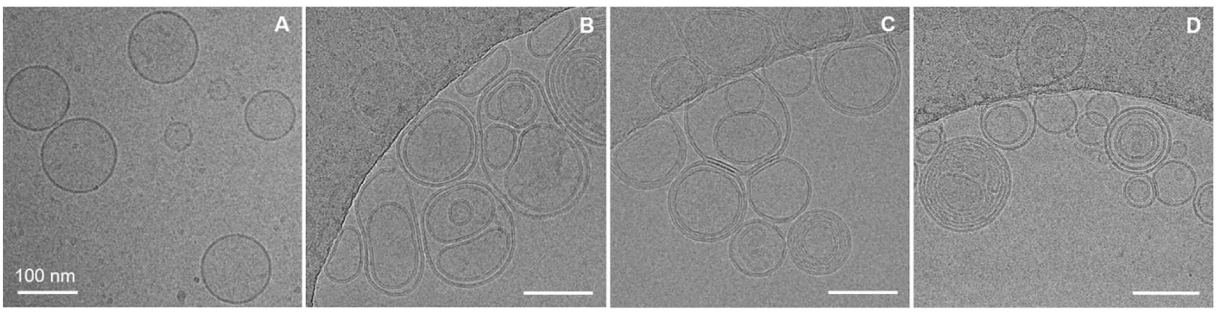

Fig. 2. Vesicles mimicking inner mitochondrial membranes. Cryo-EM images of vesicles in 200 mM NaCl with (A) IMLM+CL, (B) IMLM, (C) IMLM+PG, and (D) IMLMneutral composition. The scale bar corresponds to 100 nm.

Table 3
Solubilization of the artificial inner mitochondrial membrane vesicles using polymers of various charge at different polymer/lipid ratios.

Polymer	SMA(2:1)		DIBMA		Glyco-DIBMA		SB-DIBMA		QA1-SMA(2:1)		QA2-SMA(2:1)	
Polymer charge	−2		−2		−1		±0		+1		+1	
m_P/m_L (g/g)	c_{NaCl} (mM)											
	200	500	200	500	200	500	200	500	200	500	200	500
0.25								×				
0.5								×				
1					×	×	×	×				
1.5					×	×	×	×				
5		×			×	×	×	×				
10	×	×	×	×	×	×	×	×		×		×

P = polymer, L = IMLM+CL.

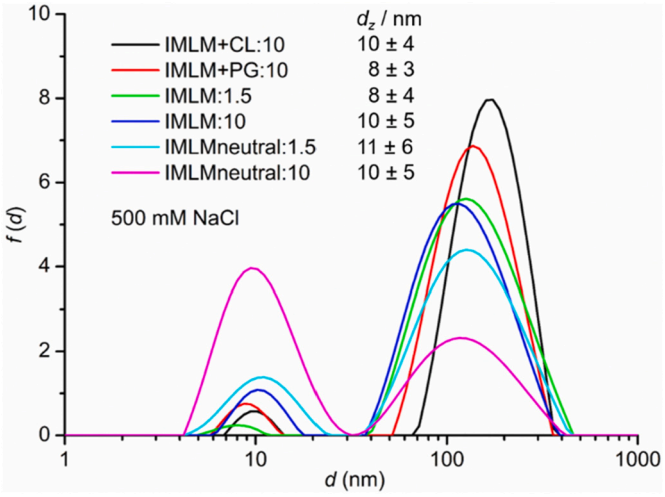

Fig. 3. DIBMA-NDs of artificial inner mitochondrial lipid mixtures. Intensity-weighted particle size distributions, $f(d)$, of IMLM+CL (m_P/m_L = 10), IMLM+PG (10), IMLM (1.5, 10), and IMLMneutral (10) at 500 mM NaCl, as obtained from DLS.

high polydispersity of the samples, since all solubilization samples contained remaining vesicles (Fig. 3). This polydispersity is also reflected in the EM images (Fig. 4), where NDs as well as vesicles are visible (Fig. 4C, D). We will show later one example of a detailed size distribution analysis by negative-stain EM of ~40.000 ND particles using class averages.

DLS and negative-stain EM show that the solubilization of highly charged IMLM+CL vesicles with DIBMA in the presence of 200 or 500 mM NaCl was possible only at high polymer concentrations (m_P/m_L = 10; Fig. 3, 4A, S4A, S5). The reason for this observation is most probably complex. All lipids of IMLM+CL naturally have a high abundance of poly-unsaturated acyl chains (Fig. S1), which are known to impede the solubilization process. CL and PE represent 68% of the IMLM+CL lipids showing inverted truncated cone shapes (Fig. S1) that may cause packing problems. Furthermore, 32% of the lipids (namely, CL and PI) are anionic, which causes Coulombic repulsion of the negatively charged polymer. Finally, DIBMA is known as a mild solubilization agent. In agreement with our data, Scheidelaar *et al.* have also reported difficulties in the solubilization of total polar lipid extract vesicles containing PE, PG, and CL with SMA(2:1), a rather harsh membrane-solubilizing copolymer [35]. The authors discuss the influence of unsaturated acyl chains and negative intrinsic curvature lipids (PE, CL), both of which increase the lateral pressure in the acyl chain region [58], leading to a less efficient insertion of the polymer. Furthermore, increased repulsive electrostatic interactions decrease both the rate and the efficiency of solubilization. Notwithstanding, we observed vesicle solubilization at a high polymer/lipid mass ratio of m_P/m_L = 10 irrespective of the NaCl concentration, which proves that lipid shape and saturation are important factors during solubilization even at Coulombic screening at elevated ionic strength.

It was surprising that IMLM+PG, where PG replaced CL, could be solubilized by DIBMA only at 500 mM NaCl and m_P/m_L = 10 (Figs. 3, 4B). A possible explanation for this observation could be that CL is preferentially located in the inner bilayer leaflet, whereas PG is equally distributed [56]. Therefore, IMLM+PG-vesicles have a higher surface charge than IMLM+PCL vesicles, which requires higher salt concentrations to screen the charges during solubilization. CL-depleted vesicles (IMLM) contain only 7% charged lipids (PI) and, therefore, can be

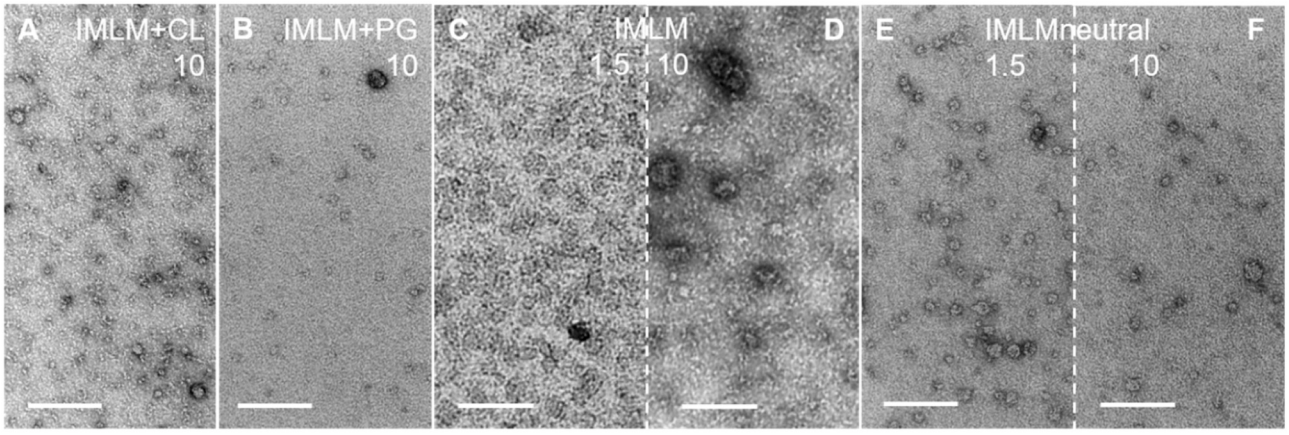

Fig. 4. DIBMA-NDs mimicking inner mitochondrial membranes. Negative-stain images of NDs in 500 mM NaCl with (A) IMLM+CL (m_P/m_L = 10), (B) IMLM+PG (10), (C, D) IMLM (1.5, 10), and (E, F) IMLMneutral (1.5, 10) composition. The scale bar corresponds to 100 nm.

solubilized at 500 mM NaCl already at very low DIBMA concentrations of $m_P/m_L = 1.5$ (Figs. 3, 4C, D), whereas at 200 mM NaCl solubilization was successful only at a considerably higher DIBMA concentration of $m_P/m_L = 10$ (Figs. S4B, S5).

3.3. Solubilization of IMLM+CL vesicles with amphiphilic copolymers of different charge

Vesicles of IMLM+CL closely mimic the lipid composition of pig heart inner mitochondrial membranes. We applied these artificial membranes to compare the solubilization efficiencies of various amphiphilic polymers, including the classical SMA(2:1) and DIBMA. In addition, polymers with either one negative charge or without negative net charge were tested (Fig. 1): Glyco-DIBMA and SB-DIBMA. Table 3 summarizes the solubilization trials on IMLM+CL at polymer/lipid mass ratios of $m_P/m_L = 0.25$, 0.5, 1, 1.5, 5, and 10, and at NaCl concentrations of 200 and 500 mM. As above, nanodisc formation was monitored by both DLS and negative stain EM (Figs. 5, 6, 7).

The solubilization of IMLM+CL vesicles required high m_P/m_L values of 10 at 200 mM NaCl for SMA(2:1) and DIBMA (see chapter 3.2.) and $m_P/m_L = 5$ at 500 mM NaCl for SMA(2:1). By contrast, positively charged QA1-SMA(2:1) and QA2-SMA(2:1) could solubilize this lipid mixture only at 500 mM NaCl. Even under these conditions, however, ND formation was not complete, as DLS indicated remaining vesicles (Fig. 5A, B).

The formed NDs showed broad size distributions between $d_z = (6 \pm 3)$ nm (QA1-SMA and QA2-SMA) and $d_z = (10 \pm 4)$ nm (DIBMA), which is also reflected in the EM images (Figs. 6, 7).

The solubilization with Glyco-DIBMA was successful at a low polymer concentration of $m_P/m_L = 1$ independent of the NaCl concentration (Table 3). DLS and EM verified the formation of NDs (Figs. 5, 6B, C, 7C, D) and showed diameters of $d_z = (10 \pm 1)$ nm up to $d_z = (19 \pm 9)$ nm. This might be due to the lower negative charge of this polymer and its hydrophilic side chains. The high polydispersity of the samples after solubilization, even at high m_P/m_L ratios, hindered a detailed discussion of the observed ND diameter.

The zwitterionic polymer SB-DIBMA showed the highest solubilization efficiency of all investigated polymers. Solubilization was successful at $m_P/m_L = 1$ in the presence of 200 mM NaCl and at $m_P/m_L = 0.25$ in the presence of 500 mM NaCl. The observed NDs were significantly smaller ($d_z = (7 \pm 3)$ nm up to $d_z = (8 \pm 4)$ nm) (Figs. 5, 6D, E, 7E, F). The efficient solubilization of highly anionic IMLM+CL vesicles by SB-DIBMA is readily explained by the complete absence of a net charge on this zwitterionic copolymer.

To validate the hydrodynamic diameters measured by DLS (Fig. 5), we used quantitative measurements and applied image analysis to electron micrographs of negatively stained samples. We focused on the SB-DIBMA/IMLM+CL-NDs ($m_P/m_L = 1$ at 200 mM NaCl) because it revealed the highest solubilization efficiency and, therefore, nanodisc yield. Representative micrographs at different applied defoci from this specimen (Fig. 8A, B) offered sufficient signal/noise ratio for quantitative analysis and statistics. As expected, even these relatively well-defined samples revealed a broad distribution of nanodisc sizes and occasionally included remaining vesicles (Fig. 8B, upper part), thus validating the above DLS results (Fig. 5A). After 2D averaging of 37,623 nanodiscs, we obtained their diameters from class averages (Fig. 8C). The diameters thus derived broadly agreed with those from DLS but, owing to the higher spatial resolution of EM as compared with DLS, also revealed a bimodal distribution of nanodisc sizes with peaks at diameter values of ~8 and ~13 nm (Fig. 8C; see below). It is also of note that NDs were, overall, not perfectly discoidal: the average minimum diameter of the class averages was ~10 nm, while the average maximum diameter amounts to ~12 nm (Fig. 8D). Examples of distinct 2D class averages of nanodiscs are also shown in Fig. 8E.

By looking into the class averages with higher ND diameters, we frequently observed side-by-side interactions between two NDs (Fig. 8F). These interactions span from long-range, possibly incidental co-localization of nanodiscs (e.g., left panel, Fig. 8F) to closer interactions (e.g., right panel, Fig. 8F). In addition, these interactions are not rare, but represent >30% of the single-particle data that were averaged (Fig. 8G), thus accounting for a considerable fraction of the larger of the two peaks in bimodal distribution of ND diameters (Fig. 8C). These larger NDs are not observed in DLS measurements, possibly due to the complexity of the measured samples. Our observation can either be attributed to incidental co-localization of nanodiscs or be likely largely only present for NDs formed by zwitterionic polymers. In this case, it is not surprising that net neutral polymers would form NDs that may undergo such interactions, aided by the absence of repulsive forces. In addition, observed ND proximity can be favored by alternate charges found in zwitterionic polymers. Most importantly, NDs have previously been shown to exchange their lipid contents rapidly with each other through collisional encounters that appear to be facilitated by the soft and flexible nature of their polymer rim. The presented data may further support this notion, as they show that NDs can engage in side-by-side interactions that are frequent and stable enough to be imaged with the aid of EM (Fig. 8F). We have recapitulated side-by-side interactions utilizing the SB-DIBMA, also shown previously by Postis et al. using SMA [59]. However, it is still unknown if this is a general trend observed for other polymers.

3.4. Solubilization of lipid vesicles mimicking inner mitochondrial membranes (S. cerevisiae) with SMA(2:1) and DIBMA

Mitochondria from different organisms deviate not only in their

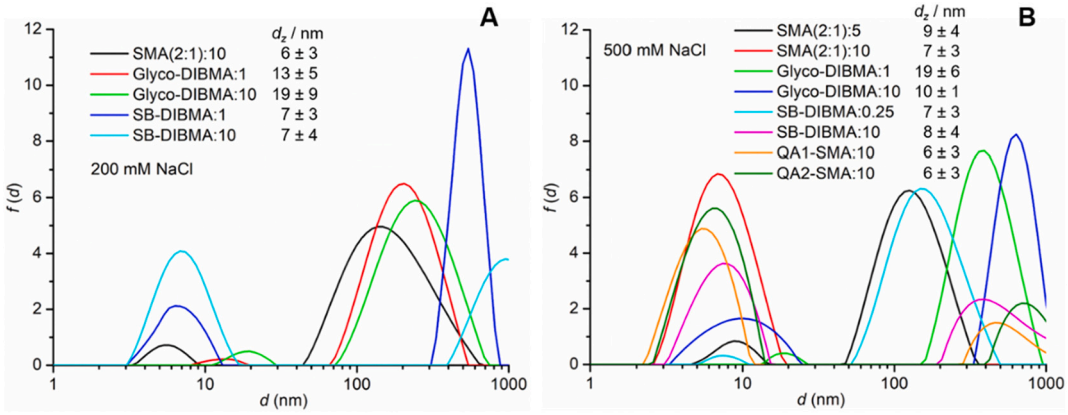

Fig. 5. Polymer/IMLM+CL-NDs mimicking inner mitochondrial membranes. Intensity-weighted particle size distributions, $f(d)$, of IMLM-NDs with SMA(2:1), Glyco-DIBMA, SB-DIBMA, QA1-SMA, and QA2-SMA at 200 (A) and 500 mM NaCl (B), as obtained from DLS.

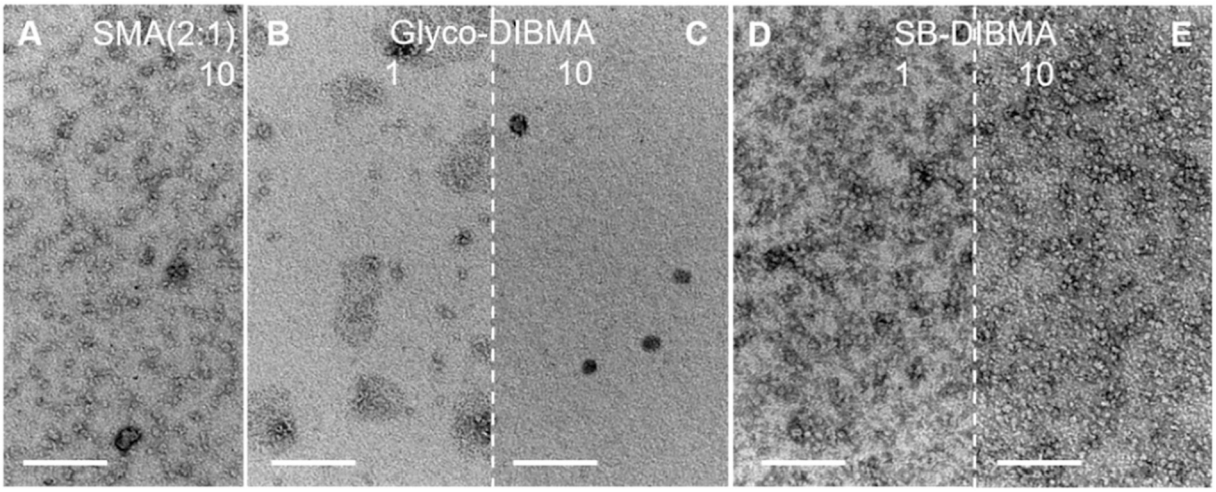

Fig. 6. Polymer/IMLM+CL-NDs mimicking inner mitochondrial membranes. Negative-stain images of NDs in 200 mM NaCl with (A) SMA(2:1) ($m_P/m_L = 10$), (B, C) Glyco-DIBMA (1, 10), and (D, E) SB-DIBMA (1, 10). The scale bar corresponds to 100 nm.

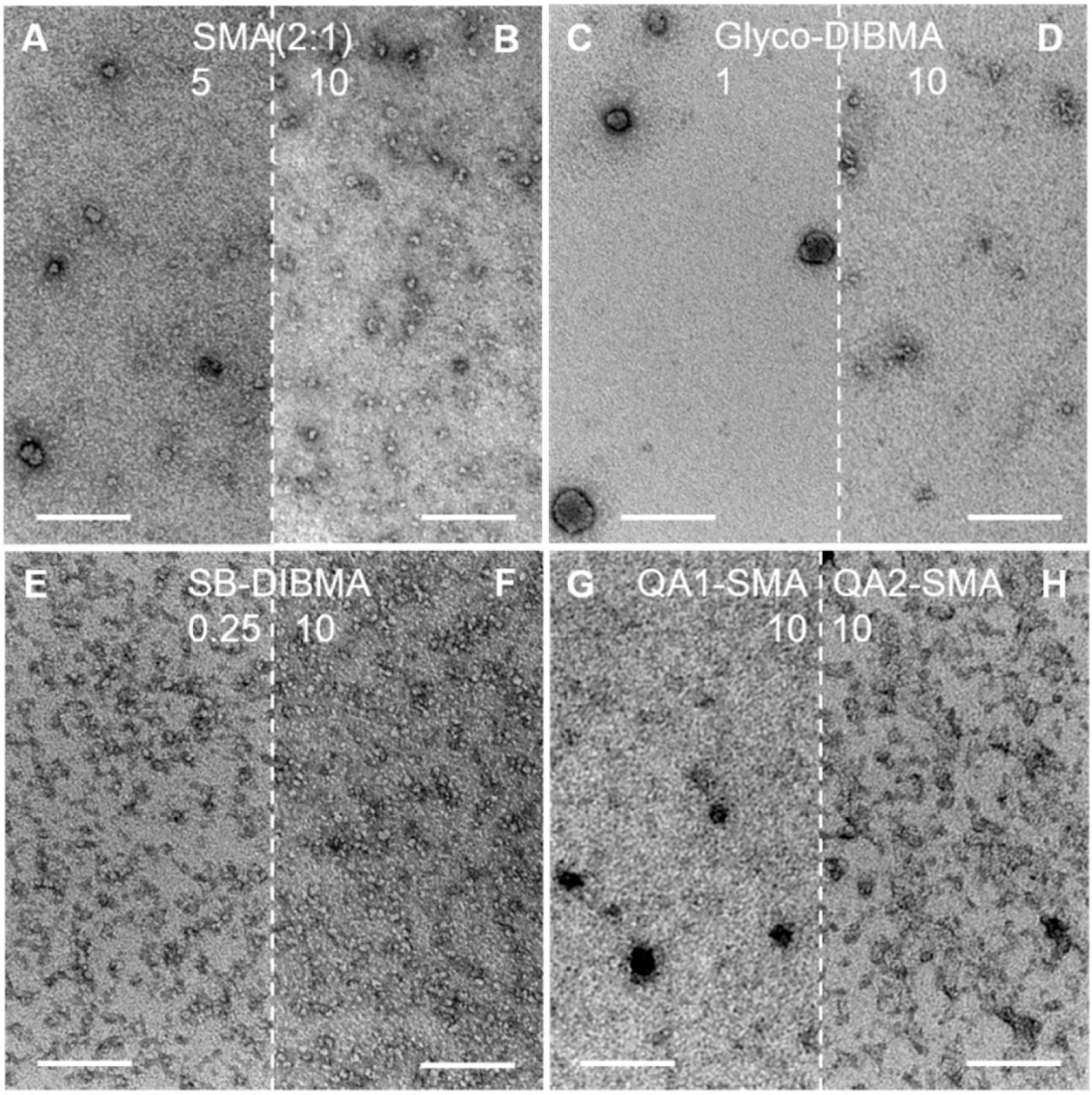

Fig. 7. Polymer/IMLM+CL-NDs mimicking inner mitochondrial membranes. Negative-stain images of NDs in 500 mM NaCl with (A, B) SMA(2:1) ($m_P/m_L = 5, 10$), (C, D) Glyco-DIBMA (1, 10), (E, F) SB-DIBMA (0.25, 10), (G) QA1-SMA (10), and (H) QA2-SMA (10). The scale bar corresponds to 100 nm.

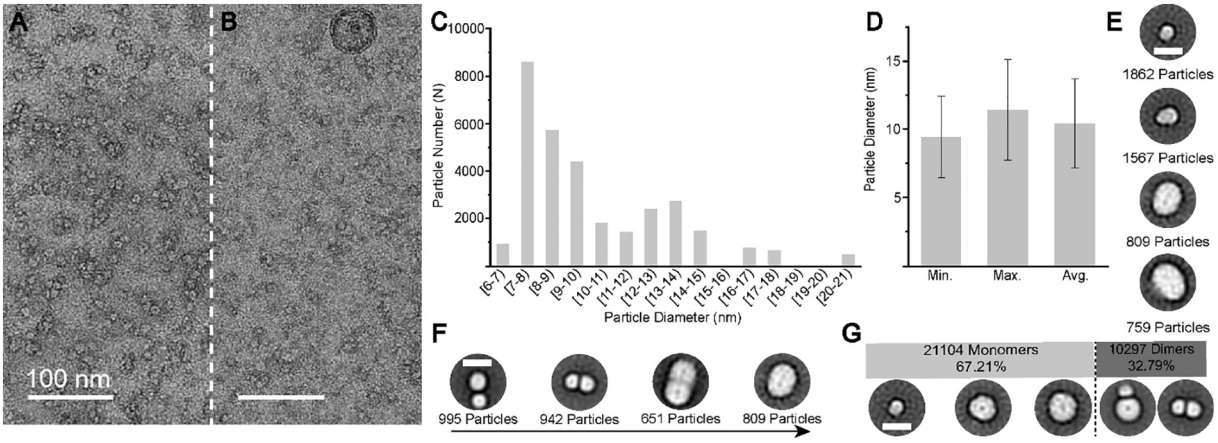

Fig. 8. Size distribution of negatively stained IMLM+CL-NDs after 2D classification. (A,B) Selected micrographs used for 2D classification. The scale bar is 100 nm. (C) Number of particles in specified particle diameter ranges. (D) Minimum, maximum, and average means of ND sizes observed. Error bars represent the mean standard deviation of the sizes, respectively. (E) Representative 2D class averages with the number of particles in each class. The scale bar is 10 nm. (F) Class averages showing side-by-side ND interactions as function of ND proximity. (G) Distribution of monomers (light gray) and dimers (dark gray) among the 2D classes (83.5% of the 37,623 NDs ended up in the analyzed classes).

macromolecular content but also, specifically, in their lipid content, especially among distinct species. The question then arises if lipid mixtures mimicking the lipid content of organism-specific mitochondria display differential solubilization behaviors. To address this question, we further investigated the solubilization of artificial *S. cerevisiae* membranes. Their inner mitochondrial lipid composition differs from the pig heart lipid mixture in that it has a lower content of CL but higher amounts of PI and in that it also contains PS. Furthermore, the acyl chain composition differs between these two artificial membranes (Figs. S1, 2, 7). Table 4 summarizes the lipid composition of the natural *S. cerevisiae* membrane and our artificial lipid composition (yeast-IMLM). The preformed extruded vesicles were smooth and partly multilamellar, as shown by cryo-EM (Fig. 9A).

Solubilization trials for yeast-IMLM at polymer/lipid mass ratios of $m_P/m_L = 0.25$, 0.5, 1, 1.5, 5, and 10 are summarized in Table 5 for NaCl concentrations of 200 and 500 mM, respectively. ND formation was monitored by DLS and negative-stain EM (Fig. 9B, C, D). Whereas DIBMA failed to solubilize yeast vesicles, SMA was able to form yeast-IMLM/SMA-NDs at $m_P/m_L = 10$ (200 mM NaCl) and $m_P/m_L = 0.25$ (500 mM NaCl), which underlines the rather harsh solubilizing character of SMA. The diameter of the NDs was $d_z = (5 \pm 2)$ nm up to $d_z = (8 \pm 3)$ nm. These results indicate that artificial mitochondrial membrane mixtures mimicking the lipid content of the same organelle membrane but from different organisms can have largely distinct behaviors during solubilization. In particular, we found CL to play a dominant role in determining the yield of nanodiscs. Specifically, lower CL contents allow membrane solubilization by SMA at lower polymer content and high salt concentrations.

Table 4
Lipid headgroup distribution of *S. cerevisiae* inner mitochondrial membrane [43] and an artificial inner mitochondrial lipid mixture (yeast-IMLM).[a]

Lipid headgroup	*S. cerevisiae* inner mitochondrial membrane		Yeast-IMLM
PC	38.4	POPC	38
PE	24.0	POPE	24
PI	16.2	POPI	16
PS	3.8	POPS	4
CL/PA	17.6	16:0–18:1 CL	18

[a] All values are given in mol%.

4. Conclusions

The motivation for our study was to compare well-established and recently developed copolymers in terms of their solubilization efficiency of CL-containing inner mitochondrial membranes. The high amount of anionic and (poly)unsaturated phospholipids and, especially, the presence of high CL amounts turned out to limit solubilization by amphiphilic copolymers. Our study aims to contribute to a better understanding of the parameters influencing the efficacy of membrane solubilization and ND formation. Since the lipid composition of natural membranes is difficult to control because of the multifaceted influences of growth conditions on cellular metabolism, we opted to create artificial membranes mimicking the lipid composition of the natural inner mitochondrial membrane of pig heart. This allowed the accurate and systematic control of lipid composition and charge during solubilization experiments. Our findings will help us and the community to produce integral and membrane-associated proteins as well as membrane-protein complexes of the inner mitochondrial membrane amenable to structural elucidation by EM without abolishing their native-like lipid environment.

Notes

Dr. Cenek Kolar is the founder and owner of Glycon Biochemicals GmbH, which sells Glyco-DIBMA. Marie Rasche is an employee of Glycon Biochemicals GmbH.

CRediT authorship contribution statement

Kevin Janson: Investigation, Analysis, Writing
Jennifer Zierath: Investigation, Analysis
Fotis L. Kyrilis: Investigation
Dmitry A. Semchonok: Investigation, Visualization
Farzad Hamdi: Investigation, Visualization
Ioannis Skalidis: Investigation
Adrian Kopf: Investigation
Manabendra Das: Conceptualization, Methodology, Investigation
Cenek Kolar: Investigation
Marie Rasche: Investigation
Carolyn Vargas: Conceptualization, Methodology, Investigation
Sandro Keller: Conceptualization, Methodology, Validation, Analysis, Funding acquisition, Resources, Writing

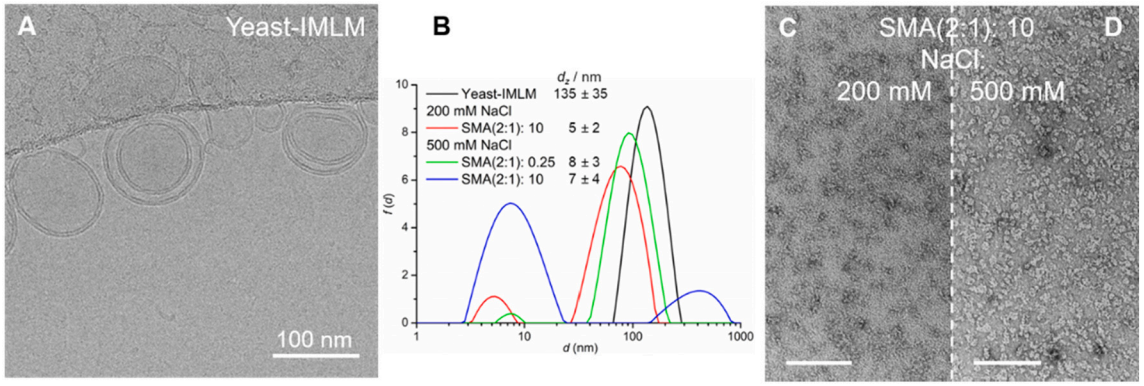

Fig. 9. SMA(2:1)/yeast-IMLM-NDs mimicking *S. cerevisiae* inner mitochondrial membranes. (A) Cryo-EM image of yeast-IMLM-vesicles in 200 mM NaCl. (B) Intensity-weighted particle size distributions, $f(d)$, of yeast-IMLM-vesicles and NDs at different m_P/m_L ratios at 200 mM NaCl and 500 mM NaCl, as obtained from DLS. Negative-stain images of NDs ($m_P/m_L = 5$) in 200 mM NaCl (C) and 500 mM NaCl (D). The scale bar corresponds to 100 nm.

Table 5
Solubilization of the artificial inner mitochondrial membrane vesicles using polymers with varying charge at different polymer to lipid ratios.

Polymer	SMA(2:1)		DIBMA	
m_P/m_L (g/g)	c_{NaCl} (mM)			
	200	500	200	500
0.25		×		
0.5		×		
1		×		
1.5		×		
5		×		
10	×	×		

P = polymer, L = yeast-IMLM.

Panagiotis L. Kastritis: Conceptualization, Methodology, Investigation, Validation, Analysis, Supervision, Funding acquisition, Resources, Writing
Annette Meister: Conceptualization, Methodology, Investigation, Validation, Analysis, Supervision, Funding acquisition, Resources, Writing.

Declaration of competing interest

The authors declare that they have no known competing financial interests or personal relationships that could have appeared to influence the work reported in this paper.

Acknowledgements

This study was funded by the Federal Ministry of Education and Research (BMBF, ZIK program) [grant numbers 03Z22HN23 and 03Z22HI2 (to P.L.K.)]; the European Regional Development Fund for Saxony-Anhalt [grant number EFRE: ZS/2016/04/78115 (to P.L.K.)], the International Graduate School AGRIPOLY supported by the European Regional Development Fund (ERDF) and the Federal State Saxony-Anhalt (A.M., P.L.K.), and the Martin Luther University Halle-Wittenberg. This work was partly funded by the Agence Nationale de la Recherche (ANR) and the DFG through the French–German FLUOR initiative (A.M.: ME 4165/2-1 and S.K.; KE 1478/7-1). This work was further supported financially by the Division of Chemical Sciences (CW) of the Netherlands Organisation for Scientific Research (NWO), via ECHO grant No. 711-017-006 (A.H.K.). We thank J.A. Killian for critical reading of the manuscript.

Appendix A. Supplementary data

Supplementary data to this article can be found online at https://doi.org/10.1016/j.bbamem.2021.183725.

References

[1] T.J. Knowles, R. Finka, C. Smith, Y.P. Lin, T. Dafforn, M. Overduin, Membrane proteins solubilized intact in lipid containing nanoparticles bounded by styrene maleic acid copolymer, J. Am. Chem. Soc. 131 (2009) 7484–7485, https://doi.org/10.1021/ja810046q.
[2] J.M. Dörr, S. Scheidelaar, M.C. Koorengevel, J.J. Dominguez, M. Schafer, C.A. van Walree, J.A. Killian, The styrene-maleic acid copolymer: a versatile tool in membrane research, Eur. Biophys. J. 45 (2016) 3–21, https://doi.org/10.1007/s00249-015-1093-y.
[3] M.C. Fiori, Y. Jiang, W. Zheng, M. Anzaldua, M.J. Borgnia, G.A. Altenberg, H. Liang, Polymer nanodiscs: discoidal amphiphilic block copolymer membranes as a new platform for membrane proteins, Sci. Rep. 7 (2017) 15227, https://doi.org/10.1038/s41598-017-15151-9.
[4] J.-L. Popot, Membrane Proteins in Aqueous Solutions, first ed., Springer Nature, Cham, 2018.
[5] R.D. Cunningham, A.H. Kopf, B.O.W. Elenbaas, B.B.P. Staal, R. Pfukwa, J. A. Killian, B. Klumperman, Biomacromolecules 21 (2020) 3287–3300, https://doi.org/10.1021/acs.biomac.0c00736.
[6] A.A.A. Smith, H.E. Autzen, B. Faust, J.L. Mann, B.W. Muir, S. Howard, A. Postma, A.J. Spakowitz, Y. Cheng, E.A. Appel, Chem 6 (2020) 2782–2795, https://doi.org/10.1016/j.chempr.2020.08.004.
[7] J.M. Dörr, M.C. Koorengevel, M. Schäfer, A.V. Prokofyev, S. Scheidelaar, E.A. van der Cruijsen, T.R. Dafforn, M. Baldus, J.A. Killian, Detergent-free isolation, characterization, and functional reconstitution of a tetrameric K+ channel: the power of native nanodiscs, Proc. Natl. Acad. Sci. U. S. A. 111 (2014) 18607–18612, https://doi.org/10.1073/pnas.1416205112.
[8] S.C. Lee, T.J. Knowles, V.L. Postis, M. Jamshad, R.A. Parslow, Y.P. Lin, A. Goldman, P. Sridhar, M. Overduin, S.P. Muench, T.R. Dafforn, A method for detergent-free isolation of membrane proteins in their local lipid environment, Nat. Protoc. 11 (2016) 1149–1162, https://doi.org/10.1038/nprot.2016.070.
[9] C. Sun, S. Benlekbir, P. Venkatakrishnan, Y. Wang, S. Hong, J. Hosler, E. Tajkhorshid, J.L. Rubinstein, R.B. Gennis, Nature 557 (2018) 123–126, https://doi.org/10.1038/s41586-018-0061-y.
[10] M. Parmar, S. Rawson, C.A. Scarff, A. Goldman, T.R. Dafforn, S.P. Muench, V.L. G. Postis, Using a SMALP platform to determine a sub-nm single particle cryo-EM membrane protein structure, Biochim. Biophys. Acta Biomembr. 1860 (2018) 378–383, https://doi.org/10.1016/j.bbamem.2017.10.005.
[11] W. Qiu, Z. Fu, G.G. Xu, R.A. Grassucci, Y. Zhang, J. Frank, W.A. Hendrickson, Y. Guo, Structure and activity of lipid bilayer within a membrane-protein transporter, Proc. Natl. Acad. Sci. U. S. A. 115 (2018) 12985–12990, https://doi.org/10.1073/pnas.1812526115.
[12] H.E. Autzen, D. Julius, Y. Cheng, Membrane mimetic systems in cryoEM: keeping membrane proteins in their native environment, Curr. Opin. Struct. Biol. 58 (2019) 259–268, https://doi.org/10.1016/j.sbi.2019.05.022.
[13] C. Sun, R.B. Gennis, Single-particle cryo-EM studies of transmembrane proteins in SMA copolymer nanodiscs, Chem. Phys. Lipids 221 (2019) 114–119, https://doi.org/10.1016/j.chemphyslip.2019.03.007.
[14] A.O. Oluwole, B. Danielczak, A. Meister, J.O. Babalola, C. Vargas, S. Keller, Solubilization of membrane proteins into functional lipid-bilayer nanodiscs using a diisobutylene/maleic acid copolymer, Angew. Chem. Int. Ed. Engl. 56 (2017) 1919–1924, https://doi.org/10.1002/anie.201610778.
[15] A.A. Gulamhussein, R. Uddin, B.J. Tighe, D.R. Poyner, A.J. Rothnie, A comparison of SMA (styrene maleic acid) and DIBMA (di-isobutylene maleic acid) for

membrane protein purification, Biochim. Biophys. Acta Biomembr. 1862 (2020), 183281, https://doi.org/10.1016/j.bbamem.2020.183281.
[16] T. Ravula, N.Z. Hardin, S.K. Ramadugu, A. Ramamoorthy, pH tunable and divalent metal ion tolerant polymer lipid nanodiscs, Langmuir 33 (2017) 10655–10662, https://doi.org/10.1021/acs.langmuir.7b02887.
[17] M. Overduin, M. Esmaili, Memtein: the fundamental unit of membrane:protein structure and function, Chem. Physics Lipids 218 (2019) 73–84, https://doi.org/10.1016/j.chemphyslip.2018.11.008.
[18] T. Ravula, N.Z. Hardin, A. Ramamoorthy, Polymer nanodiscs: advantages and limitations, Chem. Phys. Lipids 219 (2019) 45–49, https://doi.org/10.1016/j.chemphyslip.2019.01.010.
[19] J.F. Bada Juarez, A.J. Harper, P.J. Judge, S.R. Tonge, A. Watts, From polymer chemistry to structural biology: the development of SMA and related amphipathic polymers for membrane protein extraction and solubilisation, Chem. Phys. Lipids 221 (2019) 167–175, https://doi.org/10.1016/j.chemphyslip.2019.03.008.
[20] B. Danielczak, A. Meister, S. Keller, Influence of Mg2+ and Ca2+ on nanodisc formation by diisobutylene/maleic acid (DIBMA) copolymer, Chem. Phys. Lipids 221 (2019) 30–38, https://doi.org/10.1016/j.chemphyslip.2019.03.004.
[21] A. Grethen, A.O. Oluwole, B. Danielczak, C. Vargas, S. Keller, Thermodynamics of nanodisc formation mediated by styrene/maleic acid (2:1) copolymer, Sci. Rep. 7 (2017) 11517, https://doi.org/10.1038/s41598-017-11616-z.
[22] A.O. Oluwole, J. Klingler, B. Danielczak, J.O. Babalola, C. Vargas, G. Pabst, S. Keller, Formation of lipid-bilayer nanodiscs by diisobutylene/maleic acid (DIBMA) copolymer, Langmuir 33 (2017) 14378–14388, https://doi.org/10.1021/acs.langmuir.7b03742.
[23] M.M. Kostelic, A.M. Ryan, D.J. Reid, J.M. Noun, M.T. Marty, Expanding the types of lipids amenable to native mass spectrometry of lipoprotein complexes, J. Am. Soc. Mass Spectrom. 30 (2019) 1416–142510, https://doi.org/10.1007/s13361-019-02174-x.
[24] M. Tanaka, H. Miyake, S. Oka, S. Maeda, K. Iwasaki, T. Mukai, Effects of charged lipids on the physicochemical and biological properties of lipid-styrene maleic acid copolymer discoidal particles, Biochim. Biophys. Acta Biomembr. 1862 (2020), 183209, https://doi.org/10.1016/j.bbamem.2020.183209.
[25] J.J. Dominguez Pardo, J.M. Doerr, A. Iyer, R.C. Cox, S. Scheidelaar, M. C. Koorengevel, V. Subramaniam, J.A. Killian, Solubilization of lipids and lipid phases by the styrene-maleic acid copolymer, Eur. Biophys. J. 46 (2017) 91–101, https://doi.org/10.1007/s00249-016-1181-7.
[26] A. Marconnet, B. Michon, C. Le Bon, F. Giusti, C. Tribet, M. Zoonens, Solubilization and stabilization of membrane proteins by cycloalkane-modified amphiphilic polymers, Biomacromolecules 21 (2020) 3459–3467, https://doi.org/10.1021/acs.biomac.0c00929.
[27] M. Esmaili, C. Acevedo-Morantes, H. Wille, M. Overduin, The effect of hydrophobic alkyl sidechains on size and solution behaviors of nanodiscs formed by alternating styrene maleamic copolymer, Biochim. Biophys. Acta Biomembr. 1862 (2020), 183360, https://doi.org/10.1016/j.bbamem.2020.183360.
[28] M.C. Fiori, W. Zheng, E. Kamilar, G. Simiyu, G.A. Altenberg, H. Liang, Extraction and reconstitution of membrane proteins into lipid nanodiscs encased by zwitterionic styrene-maleic amide copolymers, Sci. Rep. 10 (2020) 9940, https://doi.org/10.1038/s41598-020-66852-7.
[29] R.M. Johnson, C. Fais, M. Parmar, H. Cheruvara, R.L. Marshall, S.J. Hesketh, M. C. Feasey, P. Ruggerone, A.V. Vargiu, V.L.G. Postis, S.P. Muench, V.N. Bavro, Cryo-EM structure and molecular dynamics analysis of the fluoroquinolone resistant mutant of the AcrB transporter from salmonella, Microorganisms 8 (2020) 943, https://doi.org/10.3390/microorganisms8060943.
[30] G.A. Pellowe, H.E. Findlay, K. Lee, T.M. Gemeinhardt, L.R. Blackholly, E. Reading, P.J. Booth, Capturing membrane protein ribosome nascent chain complexes in a native-like environment for co-translational studies, Biochemist 59 (2020) 2764–2775, https://doi.org/10.1021/acs.biochem.0c00423.
[31] H. Ayub, M. Clare, I. Milic, N.P. Chmel, H. Boning, A. Devitt, T. Krey, R.M. Bill, A. J. Rothnie, CD81 extracted in SMALP nanodiscs comprises two distinct protein populations within a lipid environment enriched with negatively charged headgroups, Biochim. Biophys. Acta Biomembr. 1862 (2020), 183419, https://doi.org/10.1016/j.bbamem.2020.183419.
[32] J.S. Van 't Klooster, T.Y. Cheng, H.R. Sikkema, A. Jeucken, B. Moody, B. Poolman, Periprotein lipidomes of Saccharomyces cerevisiae provide a flexible environment for conformational changes of membrane proteins, elife 9 (2020), e57003, https://doi.org/10.7554/eLife.57003.
[33] S.J. Routledge, M. Jamshad, H.A. Little, Y.P. Lin, J. Simms, A. Thakker, C. M. Spickett, R.M. Bill, T.R. Dafforn, D.R. Poyner, M. Wheatley, M., Ligand-induced conformational changes in a SMALP-encapsulated GPCR, Biochim. Biophys. Acta Biomembr. 1862 (2020), 183235, https://doi.org/10.1016/j.bbamem.2020.183235.
[34] R. Adao, P.F. Cruz, D.C. Vaz, F. Fonseca, J.N. Pedersen, F. Ferreira-da-Silva, R.M. M. Brito, C.H.I. Ramos, D. Otzen, S. Keller, M. Bastos, DIBMA nanodiscs keep alpha-synuclein folded, Biochim. Biophys. Acta Biomembr. 1862 (2020), 183314, https://doi.org/10.1016/j.bbamem.2020.183314.
[35] S. Scheidelaar, M.C. Koorengevel, J.D. Pardo, J.D. Meeldijk, E. Breukink, J. A. Killian, Molecular model for the solubilization of membranes into nanodisks by styrene maleic acid copolymers, Biophys. J. 108 (2015) 279–290, https://doi.org/10.1016/j.bpj.2014.11.3464.
[36] A.C.K. Teo, S.C. Lee, N.L. Pollock, Z. Stroud, S. Hall, A. Thakker, A.R. Pitt, T. R. Dafforn, C.M. Spickett, D.I. Roper, Analysis of SMALP co-extracted phospholipids shows distinct membrane environments for three classes of bacterial membrane protein, Sci. Rep. 9 (2019) 1813, https://doi.org/10.1038/s41598-018-37962-0.
[37] A.H. Kopf, J.M. Dörr, M.C. Koorengevel, F. Antoniciello, H. Jahn, J.A. Killian, Factors influencing the solubilization of membrane proteins from Escherichia coli membranes by styrene-maleic acid copolymers, Biochim. Biophys. Acta Biomembr. 1862 (2020), 183125, https://doi.org/10.1016/j.bbamem.2019.183125.
[38] B. Danielczak M. Rasche J. Lenz E.P. Patallo S. Weyrauch F. Mahler M.T. Agbadaola A. Meister J.O. Babalola C. Vargas C. Kolar S. Keller , A Bioinspired Glycopolymer for Capturing Membrane Proteins in Native-like Lipid-bilayer Nanodiscs, bioRxiv 01.04.2021. doi:10.1101/2021.03.31.437849.
[39] T. Ravula, N.Z. Hardin, S.K. Ramadugu, S.J. Cox, A. Ramamoorthy, Formation of pH-resistant monodispersed polymer-lipid nanodiscs, Angew. Chem. Int. Ed. Engl. 57 (2018) 1342–1345, https://doi.org/10.1002/anie.201712017.
[40] M. Schlame, M. Ren, The role of cardiolipin in the structural organization of mitochondrial membranes, Biochim. Biophys. Acta Biomembr. 1788 (2009) 2080–2083, https://doi.org/10.1016/j.bbamem.2009.04.019.
[41] N. Ikon, R.O. Ryan, R., Cardiolipin and mitochondrial cristae organization, Biochim. Biophys. Acta Biomembr. 1859 (2017) 1156–1163, https://doi.org/10.1016/j.bbamem.2017.03.013.
[42] S.E. Horvath, G. Daum, Lipids of mitochondria, Prog. Lipid Res. 52 (2013) 590–614, https://doi.org/10.1016/j.plipres.2013.07.002.
[43] E. Zinser, G. Daum, Isolation and biochemical characterization of organelles from the yeast, Saccharomyces cerevisiae, Yeast 11 (1995) 493–536, https://doi.org/10.1002/yea.320110602.
[44] J. Comte, B. Maisterrena, D.C. Gautheron, Lipid composition and protein profiles of outer and inner membranes from pig heart mitochondria. Comparison with microsomes, Biochim. Biophys. Acta 419 (1976) 271–284, https://doi.org/10.1016/0005-2736(76)90353-9.
[45] P. Hassan, S. Rana, G. Verma, Making sense of Brownian motion: colloid characterization by dynamic light scattering, Langmuir 31 (2015) 3–12, https://doi.org/10.1021/la501789z.
[46] A.N. Tikhonov, Solution of incorrectly formulated problems and the regularization method. Soviet Mathematics 4 (1963) 1035-1038. Or A.N. Tikhonov, On the solution of ill-posed problems and the method of regularization, Dokl. Akad. Nauk SSSR 151 (1963) 501–504.
[47] D.E. Koppel, Analysis of macromolecular polydispersity in intensity correlation spectroscopy: the method of cumulants, J. Chem. Phys. 57 (1972) 4814, https://doi.org/10.1063/1.1678153.
[48] M. Holzer, S. Barnert, J. Momm, R. Schubert, Preparative size exclusion chromatography combined with detergent removal as a versatile tool to prepare unilamellar and spherical liposomes of highly uniform size distribution, J. Chromatogr. A 1216 (2009) 5838–5848, https://doi.org/10.1016/j.chroma.2009.06.023.
[49] J. Zivanov, N. Takanori, B.O. Forsberg, D. Kimanius, W.J.H. Hagen, E. Lindahl, S.H. W. Scheres, New tools for automated high-resolution cryo-EM structure determination in RELION-3, elife 7 (2018), https://doi.org/10.7554/eLife.42166.
[50] S.Q. Zheng, E. Palovcak, J.-P. Armache, K.A. Verba, Y. Cheng, D.A. Agard, MotionCor2: anisotropic correction of beam-induced motion for improved cryo-electron microscopy, Nat. Methods 14 (2017) 331–332, https://doi.org/10.1038/nmeth.4193.
[51] K. Zhang, Gctf: real-time CTF determination and correction, J. Struct. Biol. 193 (2016) 1–12, https://doi.org/10.1016/j.jsb.2015.11.003.
[52] J. Schindelin, I. Arganda-Carreras, E. Frise, V. Kaynig, M. Longair, T. Pietzsch, S. Preibisch, C. Rueden, S. Saalfeld, B. Schmid, J.-Y. Tinevez, D.J. White, V. Hartenstein, K. Eliceiri, P. Tomancak, A. Cardona, Fiji: an open-source platform for biological-image analysis, Nat. Methods 9 (2012) 676–682, https://doi.org/10.1038/nmeth.2019. PMID 22743772.
[53] J.S. Harb, J. Comte, D.C. Gautheron, Asymmetrical orientation of phospholipids and their interactions with marker enzymes in pig heart mitochondrial inner membrane, Arch. Biochem. Biophys. 208 (1981) 305–318, https://doi.org/10.1016/0003-9861(81)90153-3.
[54] M. Sathappa, N.N. Alder, The ionization properties of cardiolipin and its variants in model bilayers, Biochim. Biophys. Acta Biomembr. 1858 (2016) 1362–1372, https://doi.org/10.1016/j.bbamem.2016.03.007.
[55] J.N. Israelachvili, Intermolecular and Surface Forces, Academic Press, London (UK), 2011.
[56] M.M. Elmer-Dixon, J. Hoody, H.B.B. Steele, D.C. Becht, B.E. Bowler, Cardiolipin preferentially partitions to the inner leaflet of mixed lipid large unilamellar vesicles, J. Phys. Chem. B 123 (2019) 9111–9122, https://doi.org/10.1021/acs.jpcb.9b07690.
[57] J.M. Boggs, Lipid intermolecular hydrogen bonding: influence on structural organization and membrane function, Biochim. Biophys. Acta Biomembr. 906 (1987) 353–404, https://doi.org/10.1016/0304-4157(87)90017-7.
[58] R.S. Cantor, Lipid composition and the lateral pressure profile in bilayers, Biophys. J. 76 (1999) 2615–2639, https://doi.org/10.1016/s0006-3495(99)77415-1.
[59] V. Postis, S. Rawson, J.K. Mitchell, S.C. Lee, R.A. Parslow, T.R. Dafforn, S. A. Baldwin, S.P. Muench, The use of SMALPs as a novel membrane protein scaffold for structure study by negative stain electron microscopy, Biochim. Biophys. Acta Biomembr. 1848 (2015) 496–501, https://doi.org/10.1016/j.bbamem.2014.10.018.